




Absolute-phase-shift measurement in a phase-shear-readout atom interferometerSi-Tong Yan,^{1,2,*} Jun-Jie Jiang ^{1,2,*} Lin Zhou,^{1,3,4,†} Yu-Hang Ji,¹ Chuan He,¹
Zhuo Hou ^{1,2} Biao Tang,^{1,3,4} Xi Chen,^{1,3,4} Jin Wang,^{1,3,4,‡} and Ming-Sheng Zhan ^{1,3,4}¹*State Key Laboratory of Magnetic Resonance and Atomic and Molecular Physics, Innovation Academy for Precision Measurement Science and Technology, Chinese Academy of Sciences-Wuhan National Laboratory for Optoelectronics, Wuhan 430071, China*²*School of Physical Sciences, University of Chinese Academy of Sciences, Beijing 100049, China*³*Hefei National Laboratory, Hefei 230088, China*⁴*Wuhan Institute of Quantum Technology, Wuhan 430206, China*

(Received 4 October 2023; accepted 27 November 2023; published 19 December 2023)

We demonstrate that the shear phase introduced by a tilting Raman beam in a Mach-Zehnder atom interferometer actually shifts the absolute phase, and propose how this shift can be compensated for by reference to a special point of the interference fringe. In the experiment, we obtain shear interference fringes and achieve the extraction of absolute phase corresponding to gravity acceleration. To suppress the impact of position drift on measurement accuracy, we adopt a positive and negative tilt angle alternating measurement (PNTAM) method. After using this PNTAM method, when the position drift leads to a change of 2.2×10^{-3} g, the impact of this drift on the absolute measurement value is less than 1.9×10^{-4} g. This work expands the application range of the phase shear readout based atom interferometer from the current relative or differential gravity measurement to the field of absolute gravity measurement.

DOI: [10.1103/PhysRevA.108.063313](https://doi.org/10.1103/PhysRevA.108.063313)**I. INTRODUCTION**

Since its creation 30 years ago, the atom interferometer (AI) has become an important precision measurement tool [1]. On the one hand, it is used for inertial parameter measurements such as gravity, gravity gradient, rotation, and has also been applied in fields such as metrology, mineral exploration, and navigation [2–7]; on the other hand, because of its extremely high measurement accuracy, it is also used for the measurement of fundamental physical constants and the test of fundamental physics laws [8–13].

Similar to the shear interferometer used in optics [14,15], the shear phase also enables the realization of a phase shear readout (PSR) based AI. Since the phase is extracted using spatially high-resolution shear interference fringes, the effects of atomic number fluctuation and contrast variation on the phase are drastically reduced, which lays the foundation for high-precision real-time measurement AI and has attracted more and more attention [16].

This scheme has been used in a long-baseline AI that synchronized measured gravity and rotation effects, as well as test of equivalence principle (EP) [11]. Combined with the Moiré effect, the real-time measurement properties of this scheme are also used to extend the dynamic range of gravity measurements by three orders of magnitude without loss of sensitivity [17]. This scheme is also used for rotation measurements [18,19], and multiaxis gyroscope [20]. The PSR is

a technique that is generally expected to be adopted in EP test, midfrequency gravitational wave detection, and dark matter detection in future plans [21–25].

Overall, current PSR based AIs are mainly for differential gravity measurement or gravity measurement over time. Due to the fact that the phase of the shear interference fringes depends on their position, the initial phase of AI (i.e., the phase introduced without the shear phase) needs to be calibrated in periodic interference fringes used for absolute gravity measurement. Meanwhile, the drift of the reference point will limit the accuracy of the absolute gravity measurement. In existing PSR studies, the Gaussian center of the atomic cloud is usually chosen as the reference point for phase extraction [16], and the phase at this point does not actually correspond to the initial phase shift of AI. Therefore, it is very important to calibrate the position of the initial phase-shift reference point and suppress the error caused by the drift of this point used for absolute gravity measurement in PSR based AI.

Here, we conducted a theoretical analysis of the PSR and the correction under point source approximation in AI-based gravity measurement and proposed an alternative method for measuring the shear phase introduced by the rotation of the Raman wave vector. Unlike the traditional method of extracting phase from the Gaussian center of the atomic cloud, we use the point where shear phase is not sensitive to rotation angle as the reference point to extract the absolute phase shift. We discussed the differences between absolute phase shift and Gaussian center phase shift in different application scenarios, and achieved an effective readout of the absolute phase in the PSR scheme. We used an alternating measurement of positive and negative deflection angles to suppress the influence of the benchmark position drift.

*These authors contributed equally to this work.

†lzhou@wipm.ac.cn

‡wangjin@apm.ac.cn

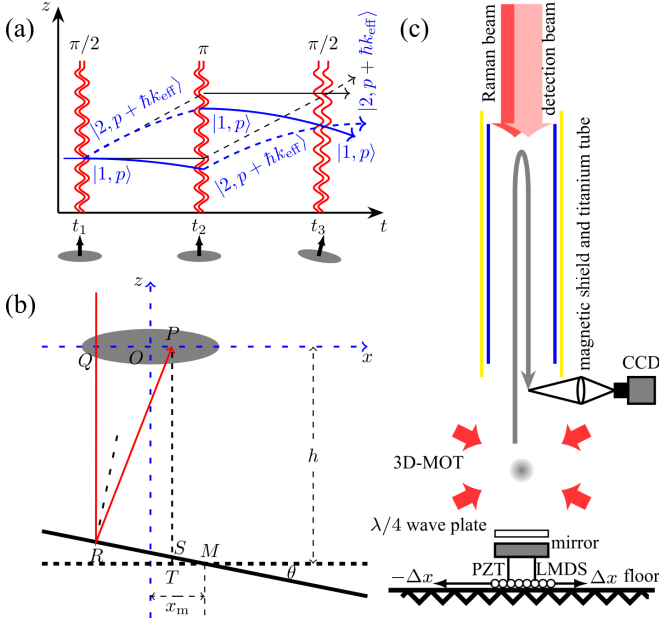


FIG. 1. (a) Space-time evolution of atoms in a Mach-Zehnder interferometer without (solid and dashed straight black lines) or with (solid and dashed curved blue lines) a constant gravitational field using PSR. Coherent Raman processes at t_1 , t_2 , and t_3 between the states $|1, p\rangle$ and $|2, p + \hbar k_{\text{eff}}\rangle$ with pulse interval of T , where the $\pi/2$, π and $\pi/2$ pulses allow for momentum transfer in the downward (solid lines) and the upward (dashed lines) directions. Note that the wave vector is tilted for the last Raman pulse, by which the shear phase is introduced. (b) The change of optical path at a spatial position P due to the tilt of the wave vector, where x_m is the horizontal distance between the Gaussian center of the atomic cloud and rotation axis of the mirror, h is the vertical distance from the mirror plane to P without mirror tilting. (c) Atoms are cooled in 3D-MOT (the horizontal cooling laser beams and 2D-MOT is not shown) and launched upward into the interference region, which is constructed with magnetic shield and titanium tube. After falling back to the detection region, the wave packets are overlapped and the interference fringe is imaged by a CCD camera

II. SCHEME OF PHASE SHEAR READOUT BASED ATOM INTERFEROMETER

In this section, we discuss the absolute phase shift of the PSR based AI. The absolute phase shift here refers to the phase of AI without the shear phase introduced, which is actually the phase shift due to gravitational acceleration. In addition, the value of gravitational acceleration can be extracted by the usual fringe scanning method [26], which we will not discuss further here.

There are two different ways to introduce shear phase in AIs: additional tilt of the wave vector of Raman laser [27] and asymmetry of the free evolution time [28]. We choose the first option to achieve the atom gravimeter. Compared to the traditional AI, the launch of atomic source, the initial state preparation and the velocity selection, as well as the first two Raman pulses interacting with the atoms in the experiment are completely the same [29]. It is only necessary to tilt the Raman beam mirror by an additional angle θ before the third Raman pulse (at t_3), as shown in Fig. 1(a).

The tilt of the Raman beam mirror with θ causes the counterpropagation Raman beams (downward and upward) to have an angle 2θ , therefore, the laser phase is delivered to the atom by the Raman beams. Since the tilt of the Raman beam mirror affects only the Raman beam (with a wave vector of k_2) that has been reflected by the mirror, we only need to consider the laser phase in this part of the optical path.

As shown in Fig. 1(b), taking the Gaussian center of the atomic cloud as the coordinate origin (the x axis of the coordinate system points to east, the y axis points to north and the z axis is vertically upward), the change of the optical path at t_3 moment at position P due to the tilt of the mirror is

$$\delta L = 2 \sin \theta [(x - x_m) \cos \theta - h \sin \theta], \quad (1)$$

where x , x_m are the horizontal coordinates of P and the rotation axis of the mirror, respectively, while h is the vertical distance from the mirror plane to P without mirror tilting.

The total phase of an AI includes ϕ_{prop} , ϕ_{sep} , and ϕ_{laser} [30], while the optical path transformation due to the mirror tilt only affects ϕ_{laser} . Since the wave vector of the Raman beam satisfies $k_{\text{eff}} \approx 2k_2$, the difference between the phase at P and the absolute phase of the AI is

$$\delta \phi = \delta \phi_{\text{laser}} \approx k_{\text{eff}} \delta L / 2. \quad (2)$$

The second-order Taylor expansion of Eq. (2) at $\theta = 0$ yields

$$\begin{aligned} \delta \phi &\approx k_{\text{eff}} \theta x - k_{\text{eff}} \theta x_m - k_{\text{eff}} h \theta^2 \\ &= \kappa_0 x - \delta \phi_L - \delta \phi_{\text{NL}}, \end{aligned} \quad (3)$$

where $\kappa_0 = k_{\text{eff}} \theta$ is the spatial frequency of atom interference fringes, the other two terms, $\delta \phi_L = k_{\text{eff}} \theta x_m$ and $\delta \phi_{\text{NL}} = k_{\text{eff}} h \theta^2$, are defined as the first- and the second-order correction terms of the phase difference between the phase at Gaussian center of the atomic cloud and the absolute phase of the AI.

Equation (3) implies that, with the mirror tilted θ , on the one hand, the atoms at different spatial positions in the direction perpendicular to the mirror rotation axis acquire an additional phase shift associated with their positions, i.e., a spatial phase gradient is introduced in the atomic cloud. On the other hand, the higher-order phase gradient is introduced in the vertical direction.

In the experiment, the detection at the end of the atom interference process is always limited by the structure of the physical system, which does not allow detection of the laser beam immediately after the third Raman pulse until the atomic cloud falls in the detection region completely, as in Fig. 1(c). Therefore, it is still necessary to consider the variation of the phase gradient at different spatial position during the time from the third Raman pulse to the detection pulse.

A. Correction of shear phase under point source approximation

Assume that the initial atomic cloud is a point source [18,27] with temperature T_a and that the velocity component v in the x direction satisfies the following distribution (the velocity distributions in y , z directions are the same):

$$f(v) = \frac{1}{\sqrt{2\pi}\sigma_v} \exp(-v^2/2\sigma_v^2), \quad (4)$$

where $\sigma_v = \sqrt{k_B T_a / m}$ is the width of the velocity distribution in the x direction, and k_B , m are the Boltzmann constant and atomic mass, respectively. The position of the atoms in the x direction during the motion starting from the launching moment until the expansion to t is completely determined by its velocity component in that direction: $x = vt$. This gives the spatial density distribution of the atoms in the x direction at the moment of detection (again, the density distributions in the y and z directions are the same)

$$n(x, t) = \frac{N}{\sqrt{2\pi}\sigma_x} \exp(-x^2/2\sigma_x^2), \quad (5)$$

where $\sigma_x = \sigma_v t$ is the width of the spatial distribution of atomic cloud at t moment and N is the total number of atoms.

From $x = vt$, the position x_3 of the atom at the moment t_3 corresponds to the position x_d at the detection moment t_d : $x_3 = x_d t_3 / t_d$. This gives the final spatial frequency of the interference fringe $\kappa_d = \kappa_0 t_3 / t_d$. Combining Eq. (5) with Eqs. (3) and (4), the spatial density distribution of atoms in a particular internal state at the moment of detection after the third Raman pulse under the point source approximation is

$$n_{ps}(x, t_d) = \frac{N}{\sqrt{2\pi}\sigma_x} \exp(-x^2/2\sigma_x^2) \times \left\{ \frac{1}{2} + \frac{C_0}{2} \cos \left[\kappa_d \left(x - x_m \frac{t_d}{t_3} \right) - k_{\text{eff}} h \theta^2 + \phi_0 \right] \right\}, \quad (6)$$

where $\phi_0 = k_{\text{eff}} g T^2$ corresponds to the phase introduced by gravity and the total phase of the AI is $\Phi = \kappa_d (x - x_m t_d / t_3) - k_{\text{eff}} h \theta^2 + \phi_0$.

It should be noted that the analyzation above discusses only the distribution perpendicular to the rotational axis of the mirror, i.e., the spatial distribution of atoms in the x direction at the moment of detection. We can use Eq. (6) to perform a least-squares fitting to the obtained shear interference fringe. The Gaussian part of the equation corresponds to the spatial distribution of the atomic cloud at the moment of detection, while the cosine part corresponds to the phase shift of the interference process. When fitting the fringe, we should first assign appropriate initial values to the fitting parameters according to the experimental parameters so that information on the phase and contrast of the interference fringe can be obtained quickly and accurately. In addition, all the phases of the AI are obtained in this way in the following experiment.

B. Phase and noise in the phase shear readout based atom interferometer

It can be seen from Eq. (3) that the noise of θ will be transferred to the total phase of the AI. We ignore the second-order correction term here for simplicity, thus the total phase of the AI should be $\Phi = \kappa_d (x - x_m t_d / t_3) + \phi_0$. Therefore, for $x = x_m t_d / t_3$, the phase at that point is exactly the same as the traditional AI, namely, $\Phi = \phi_0 = k_{\text{eff}} g T^2$. Because the phase is insensitive to tilt angle, we take this point as the absolute phase reference point. This means that the phase at $x = x_m t_d / t_3$ corresponds to gravitational acceleration and the tilt angle noise there is minimized.

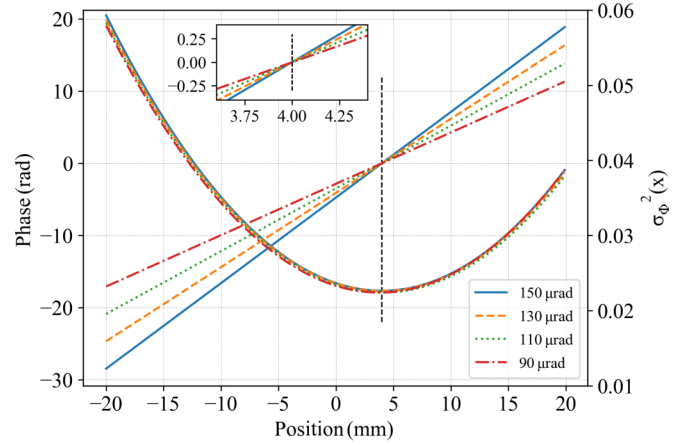


FIG. 2. Simulation of the phase and phase-noise distribution in a typical shear interference fringe. The phase varies linearly with the position in the fringe and the spatial frequency (slope of the line) also changes for different tilting angles, but there is a special position ($x = 4$ mm) where the phase of all fringes are the same. The phase noise varies quadratically with the position in the fringe, while the position of minimal phase noise is coincide with the absolute phase reference point.

We hypothesize that the noise of tilt angle θ has a normal distribution $N(\theta, \sigma_\theta)$, while the other noise of the AI is independent and has also a normal distribution, $N(0, \sigma_{\phi_0})$, thus the phase noise of the atom interference fringe gives $\sigma_\Phi^2(x) = [k_{\text{eff}} t_3 / t_d (x - x_m t_d / t_3)]^2 \sigma_\theta^2 + \sigma_{\phi_0}^2$. For a typical AI with $T = 100$ ms, we assume that the noise of the mirror tilt angle is $\sigma_\theta = 1$ μ rad, the total phase noise at different tilt angle is $\sigma_{\phi_0} = 150$ mrad (which is independent of the position in the fringe), $x_m = 2$ mm, and $t_d / t_3 = 2$, simulate the analyzation above, the results are shown in Fig. 2. It is clear that all the phase curves intersect at $x = 4$ mm, namely, the absolute phase reference point. In addition, this is also the position where the phase noise is minimized.

In our experiment, the rotation axis of the Raman beam mirror is affected by many factors, such as the imperfection of the optics, the mechanical structure of the PZT, the tilt scheme, and so on. It is difficult to accurately determine the position, so that even if the center of the Raman beam mirror and the atomic cloud are vertically aligned, it is still difficult to make the absolute phase reference point coincident with the Gaussian center of the atomic cloud. Since its phase is insensitive to different tilt angles, measurements with different tilt angles θ can be selected in the experiment, then the absolute phase reference point x_m can be obtained by fitting the phase for each measurement with Eq. (2), as in the intersection shown in Fig. 2. For the absolute gravity measurement, we extract the phase ϕ_0 at this point, then obtain the absolute gravitational acceleration value by $\phi_0 = k_{\text{eff}} g T^2$ and the corresponding analytical calculation.

C. Phase shear readout for gravity measurements

To evaluate the phase difference between the absolute phase reference point and the Gaussian center of the atomic cloud more precisely, we further discuss the phase correction

of PSR based AI in different gravity measurement scenarios on the basis of the aforementioned theoretical analysis.

According to Eqs. (3) and (6), when performing gravity measurement, the phase at different spatial position of the atomic cloud is $\Phi = \kappa_d x - \delta\phi_L - \delta\phi_{NL} + \phi_0$. Thus, the phase at the Gaussian center of the atomic cloud is not exactly ϕ_0 , but includes the first-order correction term $\delta\phi_L$ and the second-order one $\delta\phi_{NL}$.

We consider the above-mentioned effects in three aspects: the absolute gravity measurement, the gravity gradient measurement, and the EP test, respectively.

1. Absolute gravity measurement

Compared to the μGal -level absolute atom gravimeters ($1 \mu\text{Gal} = 10^{-9} \text{g}$), the currently realized gravity measurements with AIs using PSR mainly measure the relative change of gravity values over time [17]. Here, we evaluate the influences of shear phase on atom gravimeters. Taking a typical atom gravimeter as an example [26], its main parameters are $T = 200 \text{ms}$, $\theta = 120 \mu\text{rad}$, $x_m = 1.0 \text{mm}$, and $h = 50 \text{cm}$.

The ratios of $\delta\phi_L$, $\delta\phi_{NL}$ to the total phase shift of the AI are

$$\begin{aligned} \frac{\delta\phi_L}{k_{\text{eff}}gT^2} &= \frac{\theta x_m}{gT^2} = 3.1 \times 10^{-7}, \\ \frac{\delta\phi_{NL}}{k_{\text{eff}}gT^2} &= \frac{h\theta^2}{gT^2} = 1.8 \times 10^{-8}. \end{aligned} \quad (7)$$

The calculation result shows that the biggest challenge in realizing high-precision absolute gravity measurement is precisely determining the position of x_m . For μGal -level atom gravimeters, if the position of the vertical distance is controlled to $\delta h = 1.0 \text{cm}$ precisely in the term $\delta\phi_{NL}$, then the impact of the corrected value will be much less than $1 \mu\text{Gal}$, which can be realized easily. The effect of the $\delta\phi_L$ term should also be reduced to less than $1 \mu\text{Gal}$, which means that the position of x_m has to be accurate to $3 \mu\text{m}$. At the same time, the relative position of the mirror rotation axis and the imaging system in the x direction also have to be controlled or measured in real-time to this level, otherwise the relative position change of $3 \mu\text{m}$ will likewise lead to the drift of the absolute gravity value to be close to $1 \mu\text{Gal}$. In addition, the controllability of the experimental system (e.g., deformation of the experimental system due to the temperature and stress changes) determines the precision of the absolute atom gravimeter. Of course, the above requirements are only needed by extremely high-precision absolute gravimeters. For the relative gravity measurement, we need only to control the stability of the relative position. Like in a navigation atom gravimeter, its accuracy requirement is generally in the mGal level ($1 \text{mGal} = 10^{-6} \text{g}$). For an atom gravimeter works with $T = 30 \text{ms}$, even the absolute value of gravity is needed, it is relatively easy to control the position uncertainty of x_m to be less than 0.1mm , and this will ensure a measurement precision of 1.4mGal .

2. Gravity gradient measurement

The atom gravity gradiometer can be used to measure differential gravity values at different locations. In the vertical configuration case, the two AIs (above and below) of

the gravity gradiometer share the same Raman beam mirror, the gravity gradient can be obtained by making differential measurements of the shear interference fringes of the two AIs (without involving the absolute phase reference point), and considering the second-order phase correction term. For a typical atom gravity gradiometer with parameters $T = 130 \text{ms}$, $\theta = 120 \mu\text{rad}$ [31], the phase shift introduced by the separation of the atomic cloud in the vertical direction of the two AIs, δh , is

$$\delta\Gamma = \frac{\delta\phi_\Gamma}{\delta h k_{\text{eff}} T^2} = \frac{\theta^2}{T^2} = 852 \times 10^{-10} \text{g/m}, \quad (8)$$

namely, the separation of the atomic cloud in the vertical direction introduces a gradient bias $\delta\Gamma = 852 \times 10^{-10} \text{g/m}$; this can be corrected by accurately controlling θ and T .

However, in actual measurements, changes in the relative position between the mirror rotation axis and the detector in the x direction will still cause drift in measured values. If two detectors are used [31], although the atom gravity gradiometer is insensitive to the change of the mirror rotation axis, the position uncertainty of the two detectors will lead to a differential phase shift and a drift in measured value. If a single detector is used [8], according to Eq. (3), due to the different detection time between the two AIs, the variation of x_m can still be a constraint on the long-term stability. Since this effect is similar to that in absolute gravity measurements, and atom gravity gradiometers require higher accuracy in phase shift measurement, this requires that the relative position control accuracy or real-time measurement accuracy of the mirror axis and imaging system may be better than $1 \mu\text{m}$, which is much more challenging.

3. Equivalence principle test

In the AI-based EP test, the two species' atoms are perfectly simultaneously in time and in space during the entire process, the difference comes only from the detection position which can be canceled by altering the detection procedure of the two components [12]. Therefore, the phase shift introduced by the PSR scheme is essentially canceled out. Consider the EP test with four-wave double-diffraction Raman transition (4WDR) AI [32,33], due to the effective wave vector difference of the Raman lasers for ^{85}Rb and ^{87}Rb AIs, δk_{eff} , as well as the position difference in the centroid of the atomic cloud in the vertical direction, δh , the correction terms lead to phase changes. For our AI-based EP test, the typical parameters are $\delta h = 0.1 \text{mm}$, $\theta = 120 \mu\text{rad}$, $h = 2.5 \text{m}$, $\delta k_{\text{eff}}/k_{\text{eff}} = 5 \times 10^{-6}$, $T = 1.0 \text{s}$, and $x_m = 1.0 \text{mm}$, thus the ratios of $\delta\phi_L$, $\delta\phi_{NL}$ to the total interferometer phase shift are

$$\begin{aligned} \frac{\delta\phi_L}{k_{\text{eff}}gT^2} &= \frac{\delta k_{\text{eff}} x_m \theta}{k_{\text{eff}}gT^2} = 6.1 \times 10^{-14}, \\ \frac{\delta\phi_{NL1}}{k_{\text{eff}}gT^2} &= \frac{\delta k_{\text{eff}} h \theta^2}{k_{\text{eff}}gT^2} = 1.8 \times 10^{-14}, \\ \frac{\delta\phi_{NL2}}{k_{\text{eff}}gT^2} &= \frac{\delta h \theta^2}{gT^2} = 1.4 \times 10^{-13}, \end{aligned} \quad (9)$$

where $\delta\phi_{NL1}$ and $\delta\phi_{NL2}$ are the second-order correction terms caused by wave-vector difference δk_{eff} and position difference δh , respectively.

For the current AI-based EP test experiments [11–13], the phase-correction introduced by the PSR are small and can be reduced by further parameter optimization.

From the analyzation above, we can see that the phase of the shear interference fringe is correlated with the spatial position, thus it is quite sensitive to the change of position in time and space. In the EP test, due to the high coincidence of the dual-species AI in time and space, as well as the differential measurement, the advantages of the PSR scheme are fully utilized, achieving the highest accuracy measurement of the AI. However, in absolute gravity measurements and gravity gradient measurements, changes in the rotation axis and detector position in the x direction cause measurement noise and drift. Therefore, the control accuracy of position is an important factor for the measurement accuracy.

III. EXPERIMENT

We carry out the demonstration experiment with an atom gravimeter. Due to the small value of the second-order correction term and its correctability, we mainly focus on the first-order correction term. The configuration of our atom fountain is (0,1,1), i.e., the three pairs of counterpropagating laser beams orthogonal to each other that constitute the three-dimensional magneto-optical trap (3D-MOT): one pair is in the x - y plane (along the y axis and also parallel to the axis of the magnetic field coil), and the other two pairs are in the x - z plane (and symmetric with respect to the z axis) [26]. After precooling ^{85}Rb atoms in a two-dimensional magneto-optical trap (2D-MOT), the 3D-MOT was loaded with about 10^9 atoms within 1.2 s. By using moving molasses and polarization gradient cooling (PGC), an atom fountain with temperature of several μK and initial launching velocity of 3 m/s is obtained. The height of the interference region with a steady magnetic field strength is 20 cm. During the movement of the atomic cloud, three Raman pulses, $\pi/2 - \pi - \pi/2$, with a time interval of T are applied along the vertical direction, the atomic wave packet is divided, reflected, and recombined coherently to realize the Mach-Zehnder AI. Before the final $\pi/2$ pulse, the Raman beam mirror is added at an additional tilt angle θ , then the reflected Raman beam has an angle of 2θ with the vertical direction, so that the atomic cloud will obtain spatial phase gradient distribution in the horizontal direction. After the interference process, the atomic cloud falls freely to the detection region, which is 17 cm vertically above the 3D-MOT. Our detection system is mainly composed of a lens (DHC GCO-232203) and a charge coupled device (CCD) camera (ANDOR iXon Ultra 888). The ^{85}Rb atoms are exposed to the vertical detecting beam, which is resonant with the transition of $|F = 3\rangle - |F' = 4\rangle$, when they arrive straight ahead of the lens. The fluorescence is captured by the camera, thus the atoms in $|F = 3\rangle$ after interference process are imaged. The entire experimental setup is schematically shown in Fig. 1(c).

The cooling laser system is the same as described in [34], which contains a seed laser module, a TA module, an eight-pass acousto-optic frequency shift module, four frequency shift modules, and a beam splitting module. For the Raman laser system, we use an acousto-optic modulator (AOM) with a center frequency of 1.5 GHz to obtain its first-order positive

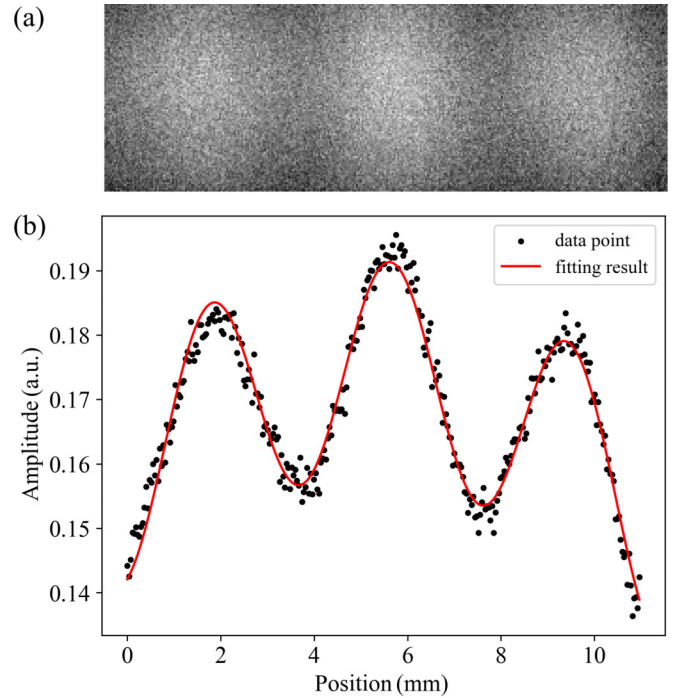


FIG. 3. (a) The image of ^{85}Rb atomic cloud ($|F = 3\rangle$) for PSR with $T = 100$ ms and $\theta = 120\ \mu\text{rad}$. (b) The shear interference fringe obtained by combining the image along the vertical direction (black dots), the phase uncertainty is 28 mrad by performing the least-squares fitting (solid red line), thus the single measurement resolution gives 1.8×10^{-8} g.

and negative diffracted beam, while the laser frequencies are ω_1 and ω_2 , respectively. The two Raman beams are combined together and adjusted to the same linear polarization, passed through another AOM with center frequency of 110 MHz, then combined with a blow-away laser beam in time-division multiplexing mode [35]. Finally, a single-mode polarization-maintaining fiber is used to guide the lasers to the beam expander at the top of the system. The expanded laser beams propagate downward vertically until being reflected by a mirror mounted at the bottom of the system. The laser beams transmit through a $\lambda/4$ wave plate twice, so as to meet the requirement of Raman beam for realizing the Doppler-sensitive Raman transition. The π pulse width is $\tau = 64\ \mu\text{s}$.

To verify the relation between the rotation axis of the Raman beam mirror and the absolute phase reference point in the shear interference fringe, we mounted the Raman beam mirror on a linear motorized displacement stage (LMDS), then we changed the position of rotation axis in x direction.

IV. RESULTS AND ANALYZATION

Figure 3(a) gives the shear interference image obtained from a single measurement in our demonstration experiment, where the free evolution time $T = 100$ ms and the Raman beam mirror tilt angle $\theta = 120\ \mu\text{rad}$. The spatial interference fringes of the atomic cloud at the moment of detection can be obtained by combining the image along the vertical direction as in Fig. 3(b). The fringe is fitted according to Eq. (6), and

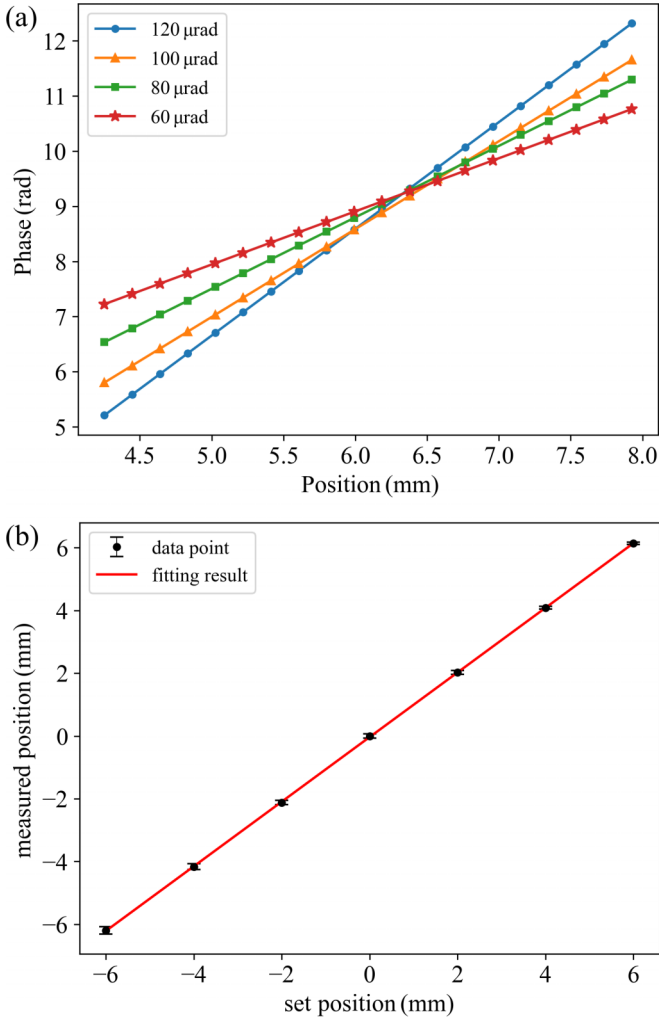


FIG. 4. (a) Curve of interference phase versus position with different tilt angles, while the intersection point, $x = 6.38$ mm, is exactly the absolute phase reference point. (b) The absolute phase reference point varies with position of the rotation axis of Raman beam mirror. The slope of line is 1.029 ± 0.002 , namely, the change of the absolute phase reference point conforms very well to the change of the rotation axis of Raman beam mirror.

the phase uncertainty is 28 mrad, thus the single measurement resolution is 1.8×10^{-8} g.

According to Eq. (6), the phase at $x = x_m t_d / t_3$ corresponds to the phase shift introduced by gravitational acceleration. Considering that $\delta\phi_L$ is independent of free evolution time T , we chose $T = 30$ ms to minimize the effect of vibration noise and to have a better demonstration of how the absolute value of the shear phase is extracted.

We first move LMDS to a position where the center of the mirror coincides as much as possible with the Gaussian center of the atomic cloud, and define this as the zero point. Then we repeat the measurements with $\theta = 60, 80, 100, 120$ μrad , respectively, and obtain the curve of the interference phase versus position, which is shown in Fig. 4(a). The intersection point in the figure is exactly the absolute phase reference point, which corresponds to a horizontal position of $x = 6.38$ mm, and is far from the Gaussian center of the atomic

cloud. This is due to the fact that there are three PZTs for the tilt platform used for two-dimensional angular adjustment of the Raman beam mirror whose internal rotation axis is difficult to be determined precisely. In addition, different tilt schemes have different rotation axes (e.g., we can obtain the same tilt angle with different tilt scheme, which corresponds to a different rotation axis), so the best way to obtain the absolute phase reference point is through the intersection point measured with different tilt angles.

When the position of the mirror is shifted along the x direction, the rotation axis of the mirror will be moved, thus the position of the absolute phase reference point in interference fringe will also be changed accordingly. For this reason, we take the zero point of the LMDS and the absolute phase reference point measured in this condition as the initial reference point for position and phase shift, respectively. Then we move the Raman beam mirror along the x direction from -6 mm to 6 mm, and use the method shown in Fig. 4(a) to measure the change of the absolute phase reference point in the interference fringe at the corresponding positions. The results are shown in Fig. 4(b). The slope of the linear fit in the figure is 1.029 ± 0.002 , the change of the absolute phase reference point conforms very well to the change of the Raman beam mirror rotation axis, while the deviation is mainly affected by the uncertainty of the amplification factor of the imaging system. Figure 4(b) also shows that the effect of the aforementioned first-order correction term can be eliminated by adjusting the position of the Raman beam mirror, so that its rotation axis coincides precisely with the Gaussian center of atomic cloud (i.e., $x_m = 0$).

In the practical applications, thermal expansion and contraction, stress and vibration noise are always unavoidable, thus it is difficult to keep the relative position of the rotation axis and the CCD camera in the x direction to 10 μm level for a long time. Also the precise experiment demands much more requirements (T is generally 10 – 100 ms in these applications, then the drift will be 10^{-6} – 10^{-8} g if the value of the gravitational acceleration is extracted in the fixed position).

To address this issue, we propose a positive and negative tilt angle alternating measurement (PNTAM) method to eliminate the influence of the drift on the final measurement result. To be specific, the shear phase is introduced by tilting the Raman beam mirror of $+\theta$ and $-\theta$ in two consecutive measurements, respectively, thus the interference phase obtained from the fitting of Eq. (6) are

$$\begin{aligned}\phi_1 &= \kappa_1(x_0 - x_m) + \phi_0, \\ \phi_2 &= \kappa_2(x_0 - x_m) + \phi_0,\end{aligned}\quad (10)$$

where x_0 is any position in the shear interference fringe, κ_i ($i = 1, 2$) is the corresponding spatial frequency of the fringe, and ϕ_i ($i = 1, 2$) is the value of the phase at that position, then we use $\phi = \kappa_{\text{eff}} g T^2$ to calculate the corresponding gravity value.

We can solve Eq. (10) to obtain the phase shift introduced by the gravitational acceleration as

$$\phi_0 = \frac{\kappa_1 \phi_2 - \kappa_2 \phi_1}{\kappa_1 - \kappa_2}.\quad (11)$$

As can be seen from Eq. (11), the phase shift introduced by the gravitational acceleration is now independent of the

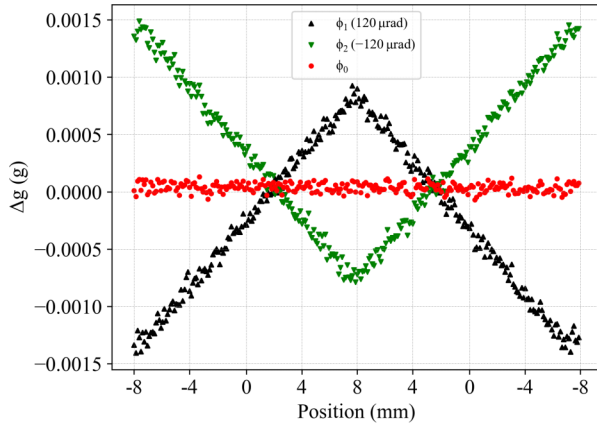


FIG. 5. Gravity measurement result using the PNTAM method. The black upper triangles and green lower triangles correspond to $\theta = 120 \mu\text{rad}$ and $\theta = -120 \mu\text{rad}$ (the result comes from the Gaussian center of the atomic cloud), respectively, and the red dots represent the result using the PNTAM method. For the position changing by 16 mm, the value of the measured gravitational acceleration is changed by $2.2 \times 10^{-3} \text{ g}$. While for PNTAM method, the values of the measured gravitational acceleration are distributed within $1.9 \times 10^{-4} \text{ g}$.

position in interference fringe. This means that the long-term drift of the system can be effectively eliminated by using this PNTAM method, as long as the relative stabilization of the mirror rotation axis to the imaging system is maintained during the two measurement processes. As discussed earlier, for $1 \mu\text{Gal}$ level absolute atom gravimeters, due to complex external environments, it is difficult to meet the requirement of keeping the relative position to an accuracy of $3 \mu\text{m}$ throughout the entire measurement process (like half a day or even longer), while this drift will similarly limit the accuracy of the atom gravity gradiometer. After using this PNTAM method, the total time of this position control accuracy is reduced to be within two measurement cycles (which will often be less than 2 s), which means that AIs using PSR are useful for high-precision measurements, such as the absolute gravimeter and gravity gradiometer, where the advantages of real-time measurement will be fully utilized.

To verify the feasibility of this scheme, we simulate the change of the rotation axis with time by continuously changing the position of the Raman beam mirror through the LMDS. The displacement platform was moved from -8 mm to 8 mm and back to -8 mm again. We solve and compare the phase shift at the Gaussian center of the atomic cloud with the phase shift calculated via Eq. (11), and the experimental results are shown in Fig. 5. The results show that when the position of the Raman beam mirror is changed, the corresponding phase at a fixed position of the interference fringe is also changed linearly. For the position changing of 16 mm, the value of the measured gravitational acceleration is changed by $2.2 \times 10^{-3} \text{ g}$. While for the PNTAM method, the values of the measured gravitational acceleration are distributed within $1.9 \times 10^{-4} \text{ g}$, and the noise mainly comes from vibration and wavefront changes caused by the moving of mirror. This means that the shear phase becomes insensitive to this position

change of rotation axis, and the change is suppressed by a factor of at least 10 in our demonstration experiment. The final accuracy of the experimental measurements is also related to factors such as the stability of the tilt angle, the resolution of the imaging system, and other experimental parameters. We believe that, after adopting this PNTAM method, practical AIs using PSR will have better performances, such as real-time measurements and normalized detection, than the existing conventional schemes, and are expected to improve the accuracy for gravity measurements.

V. SUMMARY

We analyzed the additional phase shift introduced by tilting the Raman beam mirror in a PSR based AI and proposed a method to use the angle-insensitive position as the absolute shear phase reference point. Compared with the traditional method of extracting phase from the Gaussian center of the atomic cloud, there should be a first- and second-order phase shift correction terms for this reference point. Then we quantitatively discussed the effects of the two correction terms on gravity, gravity gradient measurements, and EP test. We found that the variation in relative position between the mirror rotation axis and the detection system in the horizontal direction limits the application of PSR based AI. In the experiment, we obtained shear interference fringe with $T = 100 \text{ ms}$, and demonstrated the extraction of the absolute phase shift. By moving the position of the mirror rotation axis, we further demonstrated relation between the absolute phase reference point and the rotation axis of Raman mirror. To reduce the limitation of the measurement accuracy due to the position of the phase reference point, we proposed a PNTAM method and verified it experimentally, in which the sensitivity of the shear phase to this position change was suppressed by at least ten times.

In the future, we will suppress the phase noise of Raman beams and add a vibration isolation system so as to realize a high-precision absolute gravimeter based on PSR. Furthermore, we will carry out the accurate measurement of the second-order phase correction term. Compared with the existing method of extracting the phase shift at the Gaussian center of the atomic cloud, the method of adopting the reference point can realize the extraction of the absolute phase shift and it is insensitive to the angular noise of the tilting mirror, which is conducive to carrying out the high-precision absolute gravity measurement. The PNTAM method, on the other hand, can effectively suppress the variation of the measured gravity caused by the drift of the reference point, namely, it has better adaptability to the environment. Our work is expected to further extend the application of PSR based AI to the absolute gravity measurement, and improve the measurement stability and accuracy. In addition, these results are also useful for improving the accuracy of gravity gradient measurements and EP tests.

ACKNOWLEDGMENTS

The authors thank Yan Wang, Huanyao Sun, Qunfeng Chen, Zongyuan Xiong, Rundong Xu, and Huilin Wan for their contributions to the apparatus. This work was supported

by the Hubei Provincial Science and technology major project (Grant No. ZDZX2022000001), the Natural Science Foundation of Hubei Province (Grant No. 2022CFA096), the Chinese Academy of Sciences Project for Young Scientists in Basic

Research (Grant No. YSBR-055), National Natural Science Foundation of China (Grant No. 12174403), and the Innovation Program for Quantum Science and Technology (Grant No. 2021ZD0300603).

-
- [1] M. Kasevich and S. Chu, Atomic interferometry using stimulated Raman transitions, *Phys. Rev. Lett.* **67**, 181 (1991).
- [2] V. Ménotret, P. Vermeulen, N. Le Moigne, S. Bonvalot, P. Bouyer, A. Landragin, and B. Desruelle, Gravity measurements below 10^{-9} g with a transportable absolute quantum gravimeter, *Sci. Rep.* **8**, 12300 (2018).
- [3] K. Bongs, M. Holynski, J. Vovrosh, P. Bouyer, G. Condon, E. Rasel, C. Schubert, W. P. Schleich, and A. Roura, Taking atom interferometric quantum sensors from the laboratory to real-world applications, *Nat. Rev. Phys.* **1**, 731 (2019).
- [4] R. Geiger, V. Ménotret, G. Stern, N. Zahzam, P. Cheinet, B. Battelier, A. Villing, F. Moron, M. Lours, Y. Bidel, A. Bresson, A. Landragin, and P. Bouyer, Detecting inertial effects with airborne matter-wave interferometry, *Nat. Commun.* **2**, 474 (2011).
- [5] Y. Bidel, N. Zahzam, C. Blanchard, A. Bonnin, M. Cadoret, A. Bresson, D. Rouxel, and M. F. Lequentrec-Lalancette, Absolute marine gravimetry with matter-wave interferometry, *Nat. Commun.* **9**, 627 (2018).
- [6] F. A. Narducci, A. T. Black, and J. H. Burke, Advances toward fieldable atom interferometers, *Adv. Phys. X* **7**, 1946426 (2022).
- [7] X. Wu, Z. Pagel, B. S. Malek, T. H. Nguyen, F. Zi, D. S. Scheirer, and H. Müller, Gravity surveys using a mobile atom interferometer, *Sci. Adv.* **5**, eaax0800 (2019).
- [8] G. Rosi, F. Sorrentino, L. Cacciapuoti, M. Prevedelli, and G. M. Tino, Precision measurement of the Newtonian gravitational constant using cold atoms, *Nature (London)* **510**, 518 (2014).
- [9] R. H. Parker, C. Yu, W. Zhong, B. Estey, and H. Müller, Measurement of the fine-structure constant as a test of the Standard Model, *Science* **360**, 191 (2018).
- [10] H. Albers, A. Herbst, L. L. Richardson, H. Heine, D. Nath, J. Hartwig, C. Schubert, C. Vogt, M. Woltmann, C. Lämmerzahl, S. Herrmann, W. Ertmer, E. M. Rasel, and D. Schlippert, Quantum test of the universality of free fall using rubidium and potassium, *Eur. Phys. J. D* **74**, 145 (2020).
- [11] P. Asenbaum, C. Overstreet, M. Kim, J. Curti, and M. A. Kasevich, Atom-interferometric test of the equivalence principle at the 10^{-12} level, *Phys. Rev. Lett.* **125**, 191101 (2020).
- [12] L. Zhou, C. He, S.-T. Yan, X. Chen, D.-F. Gao, W.-T. Duan, Y.-H. Ji, R.-D. Xu, B. Tang, C. Zhou, S. Barthwal, Q. Wang, Z. Hou, Z.-Y. Xiong, Y.-Z. Zhang, M. Liu, W.-T. Ni, J. Wang, and M.-S. Zhan, Joint mass-and-energy test of the equivalence principle at the 10^{-10} level using atoms with specified mass and internal energy, *Phys. Rev. A* **104**, 022822 (2021).
- [13] B. Barrett, G. Condon, L. Chichet, L. Antoni-Micollier, R. Arguel, M. Rabault, C. Pelluet, V. Jarlaud, A. Landragin, P. Bouyer, and B. Battelier, Testing the universality of free fall using correlated ^{39}K - ^{87}Rb atom interferometers, *AVS Quantum Sci.* **4**, 014401 (2022).
- [14] M. V. R. K. Murty, The use of a single plane parallel plate as a lateral shearing interferometer with a visible gas laser source, *Appl. Opt.* **3**, 531 (1964).
- [15] H. Guan, M. Yamaguchi, and N. Ohshima, Measurement of shear in a lateral shearing interferometer, *Opt. Rev.* **2**, 285 (1995).
- [16] A. Sugarbaker, S. M. Dickerson, J. M. Hogan, D. M. S. Johnson, and M. A. Kasevich, Enhanced atom interferometer readout through the application of phase shear, *Phys. Rev. Lett.* **111**, 113002 (2013).
- [17] D. Yankelev, C. Avinadav, N. Davidson, and O. Firstenberg, Atom interferometry with thousand-fold increase in dynamic range, *Sci. Adv.* **6**, eabd0650 (2020).
- [18] G. W. Hoth, B. Pelle, S. Riedl, J. Kitching, and E. A. Donley, Point source atom interferometry with a cloud of finite size, *Appl. Phys. Lett.* **109**, 071113 (2016).
- [19] J. M. Kwolek and A. T. Black, Continuous sub-doppler-cooled atomic beam interferometer for inertial sensing, *Phys. Rev. Appl.* **17**, 024061 (2022).
- [20] Y.-J. Chen, A. Hansen, G. W. Hoth, E. Ivanov, B. Pelle, J. Kitching, and E. A. Donley, Single-source multiaxis cold-atom interferometer in a centimeter-scale cell, *Phys. Rev. Appl.* **12**, 014019 (2019).
- [21] B. Canuel, A. Bertoldi, L. Amand, E. Pozzo Di Borgo, T. Chantrait, C. Danquigny, M. Dovale Álvarez, B. Fang, A. Freise, R. Geiger, J. Gillot, S. Henry, J. Hinderer, D. Holleville, J. Junca, G. Lefèvre, M. Merzougui, N. Mielec, T. Monfret, S. Pelisson *et al.*, Exploring gravity with the MIGA large scale atom interferometer, *Sci. Rep.* **8**, 14064 (2018).
- [22] M.-S. Zhan, J. Wang, W.-T. Ni, D.-F. Gao, G. Wang, L.-X. He, R.-B. Li, L. Zhou, X. Chen, J.-Q. Zhong, B. Tang, Z.-W. Yao, L. Zhu, Z.-Y. Xiong, S.-B. Lu, G.-H. Yu, Q.-F. Cheng, M. Liu, Y.-R. Liang, P. Xu *et al.*, ZAIGA: Zhaoshan long-baseline atom interferometer gravitation antenna, *Int. J. Mod. Phys. D* **29**, 1940005 (2020).
- [23] M. Schilling, É. Wodey, L. Timmen, D. Tell, K. H. Zipfel, D. Schlippert, C. Schubert, E. M. Rasel, and J. Müller, Gravity field modelling for the Hannover 10 m atom interferometer, *J. Geod.* **94**, 122 (2020).
- [24] L. Badurina, E. Bentine, D. Blas, K. Bongs, D. Bortoletto, T. Bowcock, K. Bridges, W. Bowden, O. Buchmueller, C. Burrage, J. Coleman, G. Elertas, J. Ellis, C. Foot, V. Gibson, M. Haehnelt, T. Harte, S. Hedges, R. Hobson, M. Holynski *et al.*, AION: An atom interferometer observatory and network, *J. Cosmol. Astropart. Phys.* **05** (2020) 011.
- [25] M. Abe, P. Adamson, M. Borcean, D. Bortoletto, K. Bridges, S. P. Carman, S. Chattopadhyay, J. Coleman, N. M. Curfman, K. DeRose, T. Deshpande, S. Dimopoulos, C. J. Foot, J. C. Frisch, B. E. Garber, S. Geer, V. Gibson, J. Glick, P. W. Graham, S. R. Hahn *et al.*, Matter-wave atomic gradiometer interferometric sensor (MAGIS-100), *Quantum Sci. Technol.* **6**, 044003 (2021).
- [26] P.-W. Huang, B. Tang, X. Chen, J.-Q. Zhong, Z.-Y. Xiong, L. Zhou, J. Wang, and M.-S. Zhan, Accuracy and stability evaluation of the ^{85}Rb atom gravimeter WAG-H5-1 at the 2017

- international comparison of absolute gravimeters, *Metrologia* **56**, 045012 (2019).
- [27] S. M. Dickerson, J. M. Hogan, A. Sugarbaker, D. M. S. Johnson, and M. A. Kasevich, Multiaxis inertial sensing with long-time point source atom interferometry, *Phys. Rev. Lett.* **111**, 083001 (2013).
- [28] P. B. Wigley, K. S. Hardman, C. Freier, P. J. Everitt, S. Legge, P. Manju, J. D. Close, and N. P. Robins, Readout-delay-free Bragg atom interferometry using overlapped spatial fringes, *Phys. Rev. A* **99**, 023615 (2019).
- [29] L. Zhou, Z.-Y. Xiong, W. Yang, B. Tang, W.-C. Peng, Y.-B. Wang, P. Xu, J. Wang, and M.-S. Zhan, Measurement of local gravity via a cold atom interferometer, *Chin. Phys. Lett.* **28**, 013701 (2011).
- [30] C. Overstreet, P. Asenbaum, and M. A. Kasevich, Physically significant phase shifts in matter-wave interferometry, *Am. J. Phys.* **89**, 324 (2021).
- [31] W. Lyu, J.-Q. Zhong, X.-W. Zhang, W. Liu, L. Zhu, W.-H. Xu, X. Chen, B. Tang, J. Wang, and M.-S. Zhan, Compact high-resolution absolute-gravity gradiometer based on atom interferometers, *Phys. Rev. Appl.* **18**, 054091 (2022).
- [32] L. Zhou, S. Long, B. Tang, X. Chen, F. Gao, W. Peng, W. Duan, J. Zhong, Z. Xiong, J. Wang, Y. Zhang, and M. Zhan, Test of equivalence principle at 10^{-8} level by a dual-species double-diffraction raman atom interferometer, *Phys. Rev. Lett.* **115**, 013004 (2015).
- [33] L. Zhou, S.-T. Yan, Y.-H. Ji, C. He, J.-J. Jiang, Z. Hou, R.-D. Xu, Q. Wang, Z.-X. Li, D.-F. Gao, M. Liu, W.-T. Ni, J. Wang, and M.-S. Zhan, Toward a high-precision mass-energy test of the equivalence principle with atom interferometers, *Front. Phys.* **10**, 1039119 (2022).
- [34] R. Xu, Q. Wang, S. Yan, Z. Hou, C. He, Y. Ji, Z. Li, J. Jiang, B. Qiao, L. Zhou, J. Wang, and M. Zhan, Modular-assembled laser system for a long-baseline atom interferometer, *Appl. Opt.* **61**, 4648 (2022).
- [35] W. Yang, L. Zhou, S. Long, W. Peng, J. Wang, and M. Zhan, Time-division-multiplexing laser seeded amplification in a tapered amplifier, *Chin. Opt. Lett.* **13**, 011401 (2015).